When Do JONSWAP Spectra Lead to Soliton Gases in Deep Water Conditions?

Lee, Yu Chen; Brühl, Markus; Wahls, Sander

DOI
10.1115/OMAE2023-104326

Publication date
2023

Document Version
Final published version

Published in
Ocean Engineering

Citation (APA)
Lee, Y. C., Brühl, M., & Wahls, S. (2023). When Do JONSWAP Spectra Lead to Soliton Gases in Deep Water Conditions? In *Ocean Engineering: ASME 2023 42nd International Conference on Ocean, Offshore and Arctic Engineering* (Vol. 5). Article V005T06A101 (Proceedings of the International Conference on Offshore Mechanics and Arctic Engineering - OMAE; Vol. 5). The American Society of Mechanical Engineers (ASME). https://doi.org/10.1115/OMAE2023-104326

Proceedings of the ASME OMAE 2023 42st International & Conference on Ocean, Offshore and Arctic Engineering
OMAE2023
June 11-16, 2023, Melbourne, Australia

OMAE2023-140326

WHEN DO JONSWAP SPECTRA LEAD TO SOLITON GASES IN DEEP WATER CONDITIONS?

Yu-Chen Lee[1], Markus Brühl[2], Sander Wahls[1]

[1]Delft Center for Systems and Control, Faculty of Mechanical, Maritime and Materials Engineering, Delft University of Technology, Delft, The Netherlands
[2]Ramboll, Hamburg, Germany

ABSTRACT

When a large number of solitons dominates the dynamics of a system, scientists describe this collective behaviour of solitons as a soliton gas. Soliton gases are currently the subject of intense practical and theoretical investigations. The existence of soliton gases has been confirmed in experiments, but is not clear what kind of sea states might lead to soliton gases. Therefore, in order to determine the wave parameters for sea states that lead to soliton gases, large numbers of surface wave elevations are generated by the well-known JOSNWAP model in this paper. Here, we only discuss soliton gases in deep water governed by the nonlinear Schrödinger (NLS) equation. The nonlinear Fourier transform (NFT) with vanishing boundary conditions is applied to the simulated ocean surface waves. The resulting nonlinear Fourier spectrum is used to calculate the energy of radiation waves and solitons. We investigate which JONSWAP parameters result in sea states that can be characterized as soliton gases, and find that a large Phillip's parameter α, a large peak enhancement parameter γ and a short peak period T_p are important factors for soliton gas conditions. The results allow researchers to estimate how likely soliton gases are in deep waters. Furthermore, we find that the appearance of rogue waves is slightly increased in highly nonlinear sea states with soliton gas-like conditions.

Keywords: Nonlinear Fourier transform, Soliton gas, Deep water waves, JONSWAP spectrum

1. INTRODUCTION

Long cosine waves and undular bore-shaped waves in shallow water change into trains of solitons after travelling to the far field under certain conditions, e.g., [1, 2]. Such unsuspicious wave profiles can thus be generated by nonlinear interacting solitons. When solitons dominate the dynamics, the properties of the nonlinear wave field are characterised by interacting solitons. This scenario is known as a soliton gas in the literature.

Solitons often occur in nonlinear integrable partial differential equations (PDEs) such as the Korteweg–de Vries (KdV) equation for shallow water waves and the nonlinear Schrödinger (NLS) equation for deep water waves. The term "soliton" was first coined by Zabusky and Kruskal [3] based on numerical solutions of the KdV equation. The integrability of nonlinear PDEs enables their complete analytical solution. S-integrable PDEs can be solved by scattering transforms, which are also known as nonlinear Fourier transforms (NFTs) [4]. The S-integrability of the KdV equation was first established by Gardner et al [5]. Later, the NLS equation was solved by Zakharov and Shabat [6]. An extension of the NFT method to more PDEs was given by Ablowitz et al. [7]. Using NFTs for vanishing boundary conditions, the initial condition is transformed into a nonlinear spectrum (also called scattering data), which is composed of a continuous spectrum and a discrete spectrum. The continuous spectrum is associated with dispersive radiation waves, while the solitons are linked to the discrete spectrum. The soliton solutions for the NLS equation are envelope solitons in deep water [8]. Note that the eigenvalues in the nonlinear spectrum, which indicate the height and velocity of solitons, remain invariant during the evolution. This feature allows us to find hidden solitons in the initial condition. The collisions of NLS solitons sometimes lead to the emergence of rogue waves after propagating a certain distance [9].

Soliton gases can be described with a soliton density function. Kinetic equations describe the evolution of the soliton density function under consideration of soliton-soliton collisions, which provides a reasonable description of a soliton gas. The first kinetic equation for a rarefied soliton gas based on the KdV equation for shallow water conditions was derived by Zakharov [10]. Here, an infinite statistical ensemble of weakly interacting solitons typified by a small density of states is called a rarefied soliton gas, in contrast to the notion of a dense soliton gas. Later, the kinetic equations for a dense soliton gas for the KdV as well as for the NLS equation were obtained by El and Kamchatnov [11]. The critical density of a soliton gas was discussed by El to

Documentation for `asmeconf.cls`: Version 1.30, April 3, 2023.

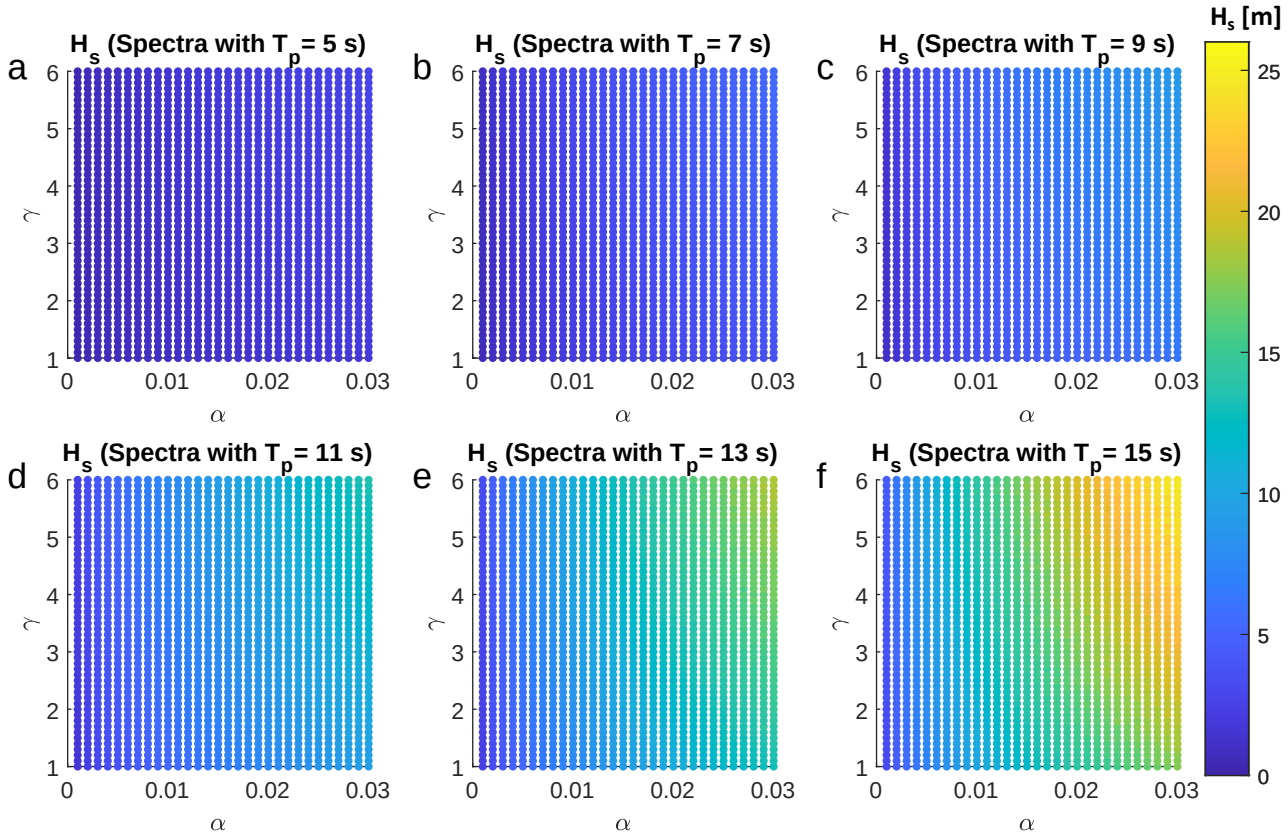

FIGURE 1: SCATTER PLOTS OF α AND γ FOR SIGNIFICANT WAVE HEIGHT OF ALL JONSWAP SPECTRA. A. SPECTRA WITH PEAK PERIOD T_p EQUAL TO 5 s. B. SPECTRA WITH PEAK PERIOD T_p EQUAL TO 7 s. C. SPECTRA WITH PEAK PERIOD T_p EQUAL TO 9 s. D. SPECTRA WITH PEAK PERIOD T_p EQUAL TO 11 s. E. SPECTRA WITH PEAK PERIOD T_p EQUAL TO 13 s. F. SPECTRA WITH PEAK PERIOD T_p EQUAL TO 15 s.

obtain a quantitative criterion for a dense soliton gas [12].

Recent numerical simulations, laboratory experiments and field measurements provide further support for the existence of soliton gases in different physical systems. Sea states that resemble a KdV-soliton gas have been measured under wind wave conditions in the Currituck Sound, North Caralina, by Costa et al. [13]. An experimental demonstration of a soliton gas in an one-dimensional wave flume has been achieved for the KdV type by Redor et al. [14] and for the NLS type by Suret et al. [15]. From the above studies, the existence of soliton gases has been confirmed in both experiments and in-situ measurements of free surface gravity waves. However, to our knowledge, there are no studies on what kind of sea states might lead to soliton gases.

In the present paper, we therefore investigate the occurrence of NLS soliton gases for unidirectional random sea states with JONSWAP spectra under deep water conditions using the NLS equation. Random realizations of specific JONSWAP spectra are generated with different values of decisive parameters, which are the peak period T_p, the Phillip's parameter α and peak enhancement parameter γ. Using the NFT for the NLS equation with vanishing boundary conditions, our analysis allows us to determine the ratio of soliton energy to total energy for each realization. From this data, we can determine how likely specific JONSWAP parameters lead to soliton gases.

The content of this paper is organized as follows. First, in Section 2, we introduce our simulation setup of surface wave data generated by JONSWAP spectra. An overview of the theoretical background of the nonlinear Fourier transform (NFT) based on the nonlinear Schrödinger (NLS) equation is presented in Section 3. Then, we directly apply the NFT on simulated data. The results are shown in Section 4, which involves an example of nonlinear Fourier analysis and an evaluation on the dominant nonlinear Fourier components in various JONSWAP sea states. The paper ends of the main conclusions in Section 5.

2. SIMULATION SETUP

The most commonly used model to describe random sea states for academic research and engineering design is according to the Joint North Sea Wave Observation Project (JONSWAP) [16]. The JONSWAP spectrum can be expressed as

$$S(f) = \frac{\alpha g^2}{(2\pi f)^5} \mathrm{e}^{-\frac{5}{4}\left(\frac{f_p}{f}\right)^4} \gamma^r, \quad \sigma = \begin{cases} 0.07 & f \le f_p \\ 0.09 & f > f_p \end{cases}, \qquad (1)$$

where $r = \exp\left[-\frac{1}{2}\left(\frac{f-f_p}{\sigma f_p}\right)^2\right]$, f is frequency, g is gravity, f_p is the dominant frequency, σ is the narrowness of the peak parameter, γ is the enhancement factor and α is the Phillip's parameter. The

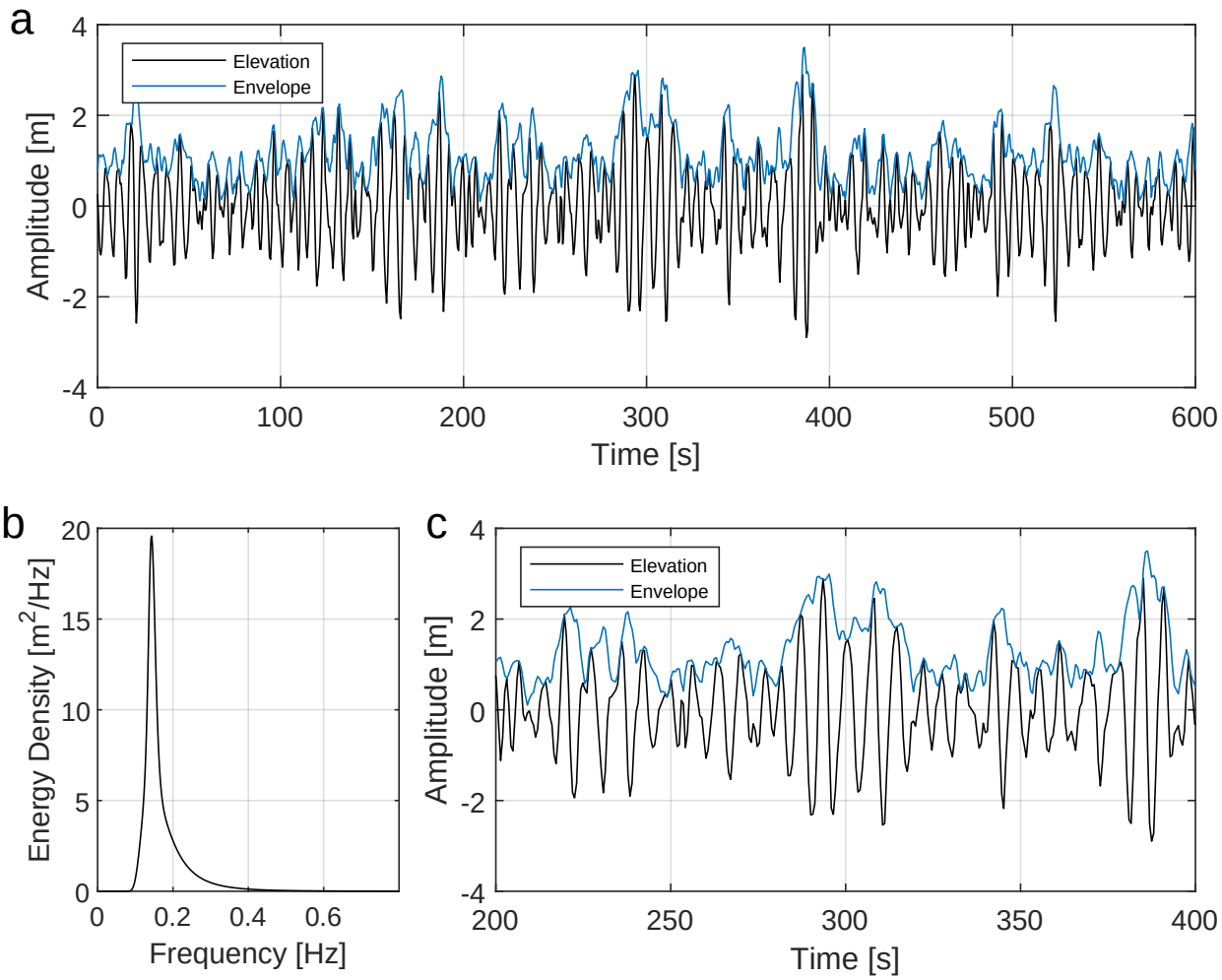

FIGURE 2: A. EXAMPLE OF A TIME SERIES OF SURFACE WAVE ELEVATION (BLACK LINE) GENERATED BY JONSWAP SPECTRUM WITH RANDOM PHASES. THE BLUE LINE REPRESENTS THE MAGNITUDE OF THE COMPLEX ENVELOPE. B. THE JONSWAP SPECTRUM WITH $f_0 = 1/7$Hz, $\alpha = 0.02$, $\gamma = 3.3$. B. ZOOM IN THE TIME SERIES OF SURFACE WAVE ELEVATION FROM 200 s TO 400 s.

parameter γ influences the peak shape. If $\gamma > 1$, the sea states are undeveloped, due to nonlinear wave-wave interactions, do not arrive at steady conditions. The higher values of enhancement factor γ represent higher and narrower in the center of the spectral peak of JONSWAP spectrum. The values of Phillip's parameter α determine the energy scale of JONSWAP spectrum.

In this study, we generated various JONSWAP spectra based on the basic JONSWAP spectral parameters α, γ and peak period T_p. The selected range of JONSWAP parameters for α is from 0.001 to 0.03 with an interval of 0.001, for γ is from 1 to 6 with an interval of 0.1, and for T_p is from 5 s to 15 s with an interval of 2 s. In total, there are 9180 JONSWAP spectra in our study. After generating JONSWAP spectra with selected JONSWAP parameters, the significant wave height H_s can be calculated from $4\sqrt{m_0}$, where m_0 is zeroth-order spectral moment. Fig. 1 shows the plots of H_s over the JONSWAP parameters α and γ. Spectra with different peak periods from 5 s to 15 s are shown from Fig. 1a to Fig. 1f. With regards to higher values of α and γ, the spectra have larger H_s due to the larger amplitude scale and sharper spectral peak.

Here, we generate two sets of surface wave data, with a time duration of 600 s and 1200 s, respectively. For each JONSWAP spectrum, we produce 10 surface elevation time series from random phases. Consequently, each resulting data set contains 91800 time series. The sampling frequency of the data is set to 1.7 Hz. We check that the time series do not exceed the wave breaking criterion. The complex envelope, which is what the NLS equation actually describes, can be calculated from the surface wave elevations with the help of the Hilbert transform [17]. The NLS-NFT analysis of the complex envelope is explained in the next section. The water depth is set to 1000 m. All simulated surface waves satisfy the critical depth $k_0 h > 1.363$ that is required for the NLS equation to be in the soliton-supporting focusing regime.

Before we start on our analysis, we would like to emphasize that our dataset of the simulated JONSWAP sea states differs from realistic sea states. Real-world spectra are complex and change

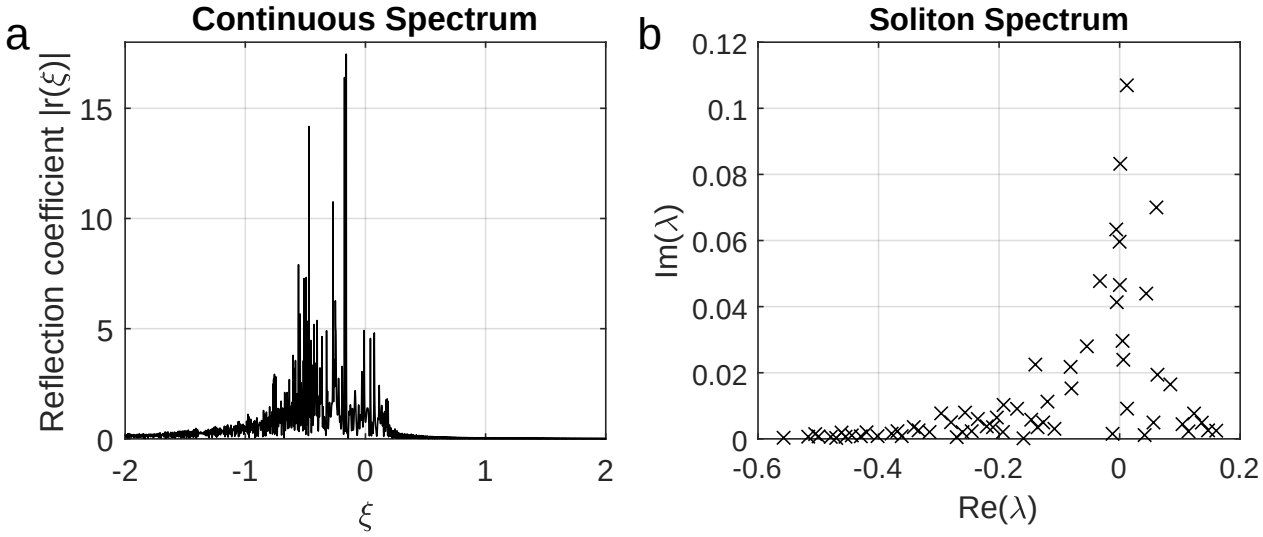

FIGURE 3: THE NON-LINEAR SPECTRUM IS DIVIDED INTO TWO PARTS: A. THE CONTINUOUS SPECTRUM AND B. THE SOLITON SPECTRUM.

from site to site with the meteorological and oceanographic conditions. However, long-term measurements of in-situ data are rare and costly. JONSWAP spectrum is commonly used to calculate the basic wave parameters for engineering design. Our data cover a wide range of JONSWAP parameters containing most of possible JONSWAP sea states from normal to extreme conditions.

3. THEORETICAL BACKGROUND

Normalization of the Nonlinear Schördinger Equation

The following description of the normalization process follows the exposition in [18].

The nonlinear Schrödinger equation is a fundamental model for nonlinear phenomena under narrow-band and unidirectional conditions, e.g. in deep water and optical fibre. The spatial NLS equation for wave field in deep water can be written as

$$i\left[A_t + C_g A_x\right] + \mu A_{tt} + \nu|A|^2 A = 0, \tag{2}$$

where $A(x,t)$ is the complex wave amplitude at location x and time t, μ is the coefficient of the second-order dispersion term and ν is the coefficient of the cubic nonlinear term. The subscripts x and t indicate partial derivatives with respect to these variables. The coefficients for surface water waves are provided in the literature [19, 20]. The coefficient ν is positive in the focusing case, which admits bright solitons as solutions [21]. For deep water waves in infinite water depth, the values of the coefficients are

$$C_g = \frac{\omega_0}{2k_0}, \quad \mu = -\frac{\omega_0}{8k_0^2}, \quad \nu = -\frac{\omega_0 k_0^2}{2}, \tag{3}$$

where C_g is the group velocity and ω_0 is the angular peak frequency, and k_0 is the wave number. For finite water depth h, the coefficients have been derived by Hasimoto and Ono [20].

The analysis of surface wave data is frequently considered in the time domain. Thus, a temporal NLS equation is needed. The transformation from the spatial NLS equation into the temporal NLS equation can be found in Refs. [18, 22], and leads to

$$i\left[C_g^{-1}A_t + A_x\right] + \mu C_g^{-3}A_{tt} + \nu C_g^{-1}|A|^2 A = 0. \tag{4}$$

For the KdV-NFT, the impact of this transformation has been investigated in [2] for specific bores. The normalized form of the NLS equation is often used in order to simplify numerical methods for the NFT. Here, we use the normalization

$$X = \frac{\mu}{C_g^3}x, T = t - \frac{x}{C_g}, u(X,T) = \rho A(X,T), \rho := \sqrt{\frac{C_g^2 \nu}{2\mu}}, \tag{5}$$

where $u(X,T)$ is the scaled envelope and ρ is the nonlinear parameter. Finally, we obtain the temporal NLS equation in normalized form:

$$iu_X + u_{TT} + 2|u|^2 u = 0. \tag{6}$$

Nonlinear Fourier Transform for Vanishing Boundary Conditions

The nonlinear Fourier transform (NFT) is used to solve the NLS equation based on the integrability of the Zakharov-Shabat system [6, 7, 23]. The form of the NFT depends on the boundary conditions. Vanishing boundary conditions are the more common choice for the NLS equation. While periodic boundary conditions may seem more appropriate than vanishing boundary conditions, the periodic NFT is more difficult to compute. Moreover, except at the boundaries of a periodic domain, it makes little difference in practice which of the two approaches one uses to detect solitons. For the Korteweg-de Vries equation this has e.g. been confirmed in [24, Fig. 11] and [2, Fig. 17]. The direct spatial evolution of the complex envelope governed by the NLS equation can be complicated. The advantage of the NFT is that the evolution of nonlinear Fourier components is very simple. One can apply the inverse nonlinear Fourier transform (iNFT) to the propagated spectrum to obtain the solution at other points in space [25].

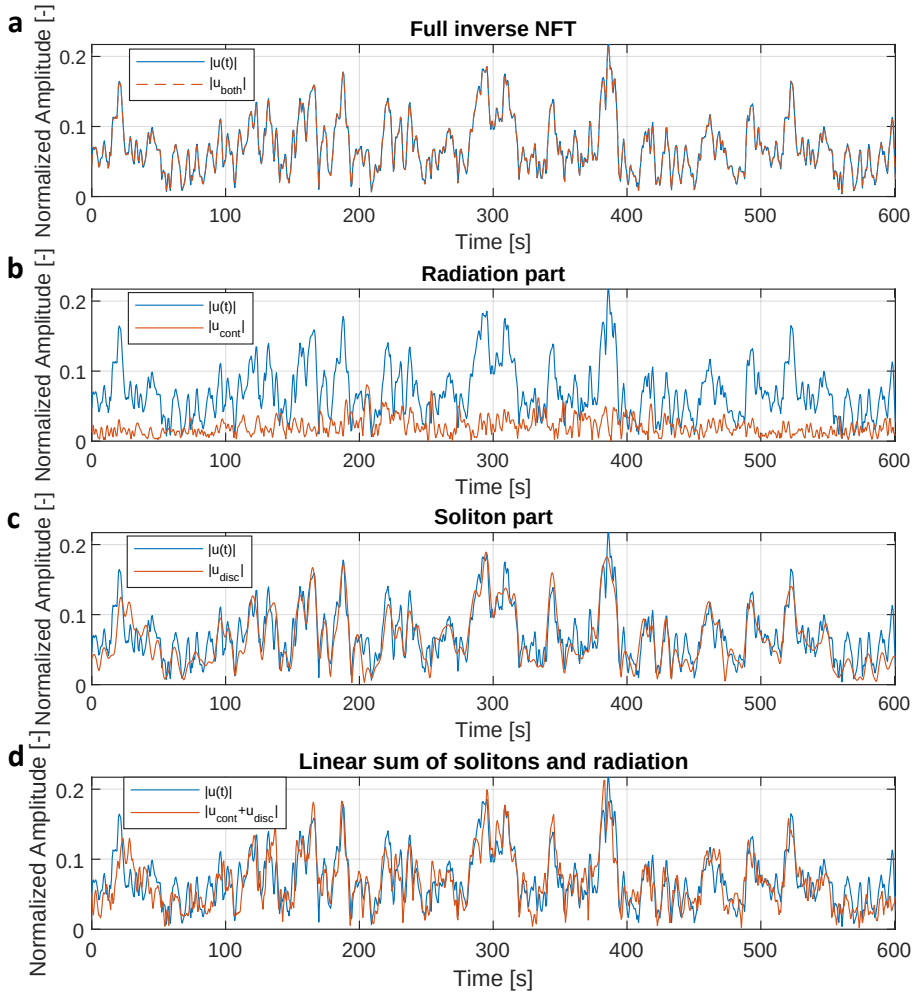

FIGURE 4: COMPARISON BETWEEN THE INITIAL SIGNAL AND THE COMPLEX ENVELOPE OF NONLINEAR SPECTRUM RECOVERED FROM THE INFT. THE BLUE LINE REPRESENTS THE INITIAL ENVELOPE IN FIG. 2. A. TIME SERIES CALCULATED FROM THE NONLINEAR SUM OF RADIATION SPECTRUM AND SOLITON SPECTRUM BASED ON THE INVERSE NONLINEAR FOURIER TRANSFORM. B. TIME SERIES CALCULATED FROM THE RADIATION SPECTRUM. C. TIME SERIES CALCULATED FROM THE SOLITON SPECTRUM. D. TIME SERIES CALCULATED FROM THE LINEAR SUM OF TIME SERIES CORRESPONDING TO ONLY THE RADIATION SPECTRUM AND ONLY SOLITON SPECTRUM.

We now discuss how the nonlinear spectrum is computed. The scattering problem for the NLS equation is

$$\Psi_T = Q(\zeta)\Psi, \quad Q = \begin{pmatrix} -i\zeta & u(X_0,T) \\ -u(X_0,T)^* & i\zeta \end{pmatrix}, \tag{7}$$

where ζ is the complex spectral parameter, and * represents complex conjugation. Two pairs of linearly independent Jost functions $[\phi(T,\zeta) \quad \bar{\phi}(T,\zeta)]$ and $[\psi(T,\zeta) \quad \bar{\psi}(T,\zeta)]$ are found by solving Eq. (7). The Jost functions are defined as

$$\begin{aligned} &\phi(T,\zeta) \to \begin{bmatrix} e^{-i\zeta T} \\ 0 \end{bmatrix}, \ \bar{\phi}(T,\zeta) \to \begin{bmatrix} 0 \\ -e^{i\zeta T} \end{bmatrix} \quad \text{as} \quad T \to -\infty, \\ &\psi(T,\zeta) \to \begin{bmatrix} 0 \\ e^{i\zeta T} \end{bmatrix}, \ \bar{\psi}(T,\zeta) \to \begin{bmatrix} e^{-i\zeta T} \\ 0 \end{bmatrix} \quad \text{as} \quad T \to \infty. \end{aligned} \tag{8}$$

The above pairs of functions are related through the scattering coefficients $a(\zeta)$, $b(\zeta)$, $\overline{a}(\zeta)$, $\overline{b}(\zeta)$:

$$\begin{aligned} \phi(T,\zeta) &= a(\zeta)\bar{\psi}(T,\zeta) + b(\zeta)\psi(T,\zeta), \\ \bar{\phi}(T,\zeta) &= \bar{b}(\zeta)\bar{\psi}(T,\zeta) + \bar{a}(\zeta)\psi(T,\zeta). \end{aligned} \tag{9}$$

The scattering coefficients $a(\zeta)$ and $b(\zeta)$ are the basis for forming the nonlinear spectrum. The nonlinear spectrum has two components: the continuous spectrum and discrete spectrum. The continuous spectrum is described by the *reflection coefficient*

$$r(\zeta) = b(\zeta)/a(\zeta), \quad \zeta \in \mathbb{R}. \tag{10}$$

It represents the radiation components in the time series. The discrete spectrum contains the discrete eigenvalues $\{\zeta_k = \xi_k + i\eta_k\}$, $k = 1, ..., N$, where N is the total number of solitons in the signal. They are the zeros of the scattering coefficient $a(\zeta)$ with positive imaginary part. The eigenvalues are complemented by

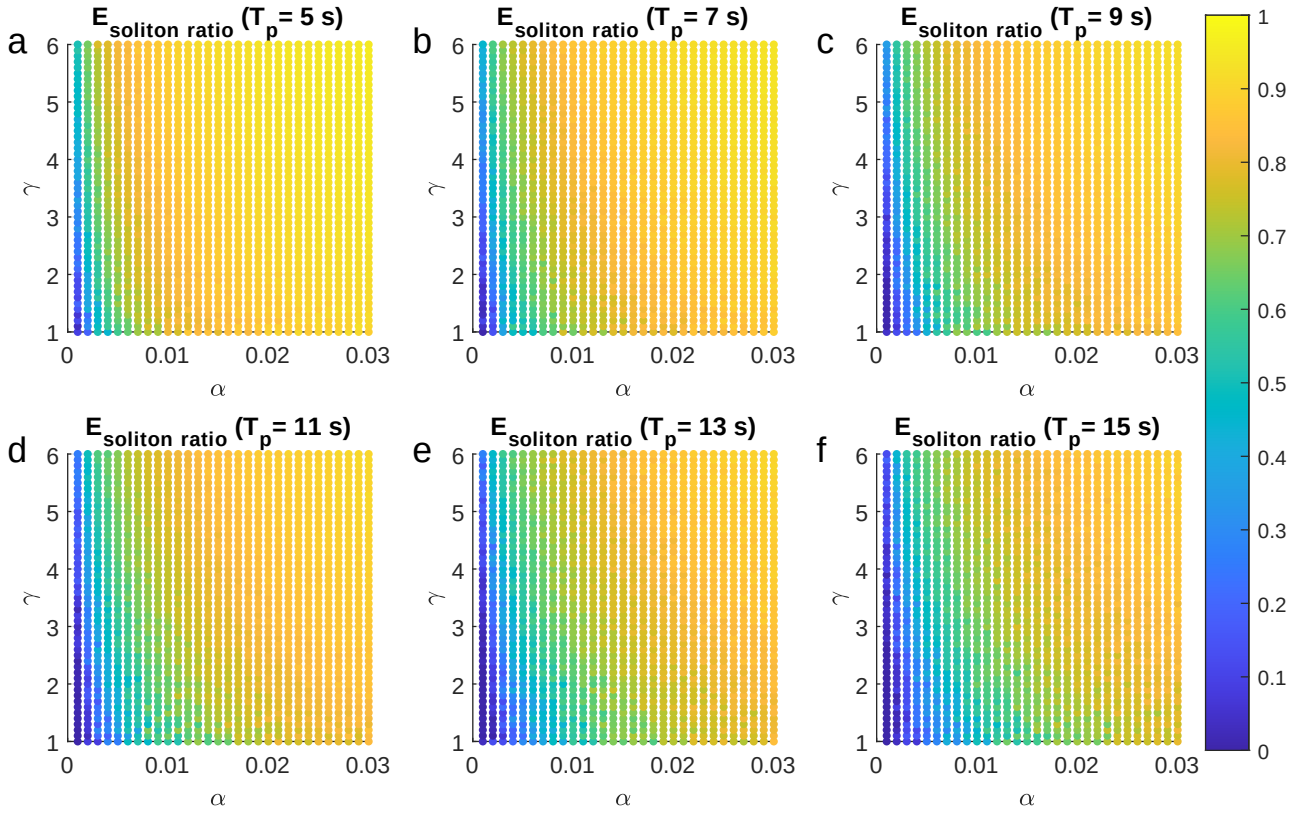

FIGURE 5: SOLITON ENERGY RATIO OVER α AND γ BASED ON THE NONLINEAR ANALYSIS OF SURFACE WAVES WITH A TIME DURATION OF 600 s FOR DIFFERENT PEAK PERIODS T_p

the residues

$$r_k = b(\zeta_k)/a'(\zeta_k), \quad \text{where} \quad a' = da/d\zeta. \tag{11}$$

The discrete spectrum corresponds to the soliton components.

Inverse Nonlinear Fourier Transform

The inverse nonlinear Fourier transform (iNFT) recovers the time domain signal from the nonlinear spectrum. This is classically achieved by using the Gelfand-Levitan-Marchenko equation (GLME) [7, 23, 26]

$$\begin{aligned} K_2^*(T,S) + \int_T^\infty K_1(T,s)F(s+S)ds = 0, \\ K_1(T,S) - \int_T^\infty K_2^*(T,s)F^*(s+S)ds = F^*(T+S), \end{aligned} \tag{12}$$

where the integral kernel $F(T)$ is given as

$$F(T) = \frac{1}{2\pi}\int_{-\infty}^{\infty} r(\zeta,T)e^{i\zeta T}d\zeta - i\sum_{k=1}^{N} r_k(T)e^{i\zeta T}. \tag{13}$$

Finding $K(T,S)$ by solving the GLME, enables us to recover a complex envelope in the time-space domain

$$u(X_0,T) = -2K_1(T,T) \tag{14}$$

More information about the inverse nonlinear Fourier transform (iNFT) can be found in the Refs. [6, 7, 23].

Soliton Energy Ratio

The energy of solitons and radiation waves can be calculated by discrete spectra and continuous spectra [23]. First, the total energy of the time series is

$$E_{\text{total}} = E_{\text{sol}} + E_{\text{rad}} = \int_{-\infty}^{\infty} |u|^2 dt, \tag{15}$$

where E_{sol} is the energy of the solitons,

$$E_{\text{sol}} = 4\sum_{k=1}^{N} \text{Im}\,(\zeta_k), \tag{16}$$

and E_{rad} is the energy of the radiation waves,

$$E_{\text{rad}} = 4\int_{-\infty}^{\infty} \log(1+|r(\zeta)|^2)d\zeta. \tag{17}$$

The soliton energy ratio is defined as

$$E_{\text{sol\_ratio}} = E_{\text{sol}}/E_{\text{total}} = (E_{\text{total}} - E_{\text{rad}})/E_{\text{total}}. \tag{18}$$

If the energy ratio is high, the solitons are the dominant components in the time series. We use the formula that utilizes the radiation energy to compute the energy ratio because it is easier to compute the continuous spectrum numerically.

Based on the soliton energy ratio, we classify the sea states into four types, as shown in Table 1: (1) If $E_{\text{sol\_ratio}} < 40\%$,

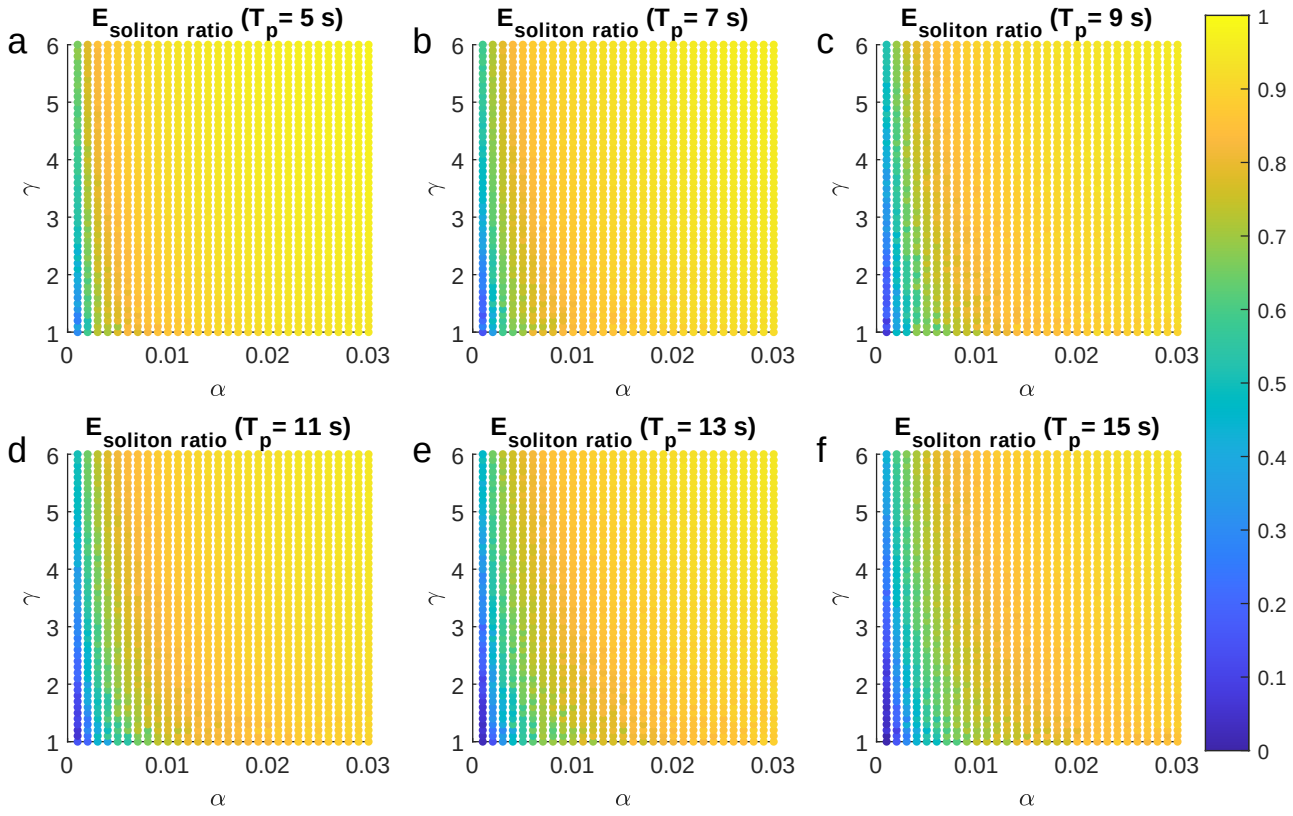

FIGURE 6: SOLITON ENERGY RATIO OVER α AND γ BASED ON THE NONLINEAR ANALYSIS OF SURFACE WAVES WITH A TIME DURATION OF 1200 s FOR DIFFERENT PEAK PERIODS T_p

the sea state is considered to be dominated by radiation waves. (2) If $40\% \leq E_{\text{sol\_ratio}} < 60\%$, the sea state is considered to be equally influenced by radiation waves and solitons. (3) If $60\% \leq E_{\text{sol\_ratio}} < 90\%$, the sea state is considered to be dominated by solitons. (4) If $90\% \leq E_{\text{sol\_ratio}} < 100\%$, the sea state is considered to be soliton gas-like.

In this study, the numerical computation of the NFTs and iNFT was performed using version 0.4.1 of the software library FNFT [27]. The routine *mex_fnft_nsev* transfers a signal in the space or time domain to the corresponding a continuous spectrum and a discrete spectrum in the nonlinear frequency domain. The routine *mex_fnft_nsev_inverse* is for the inverse nonlinear Fourier transform (iNFT).

An example of nonlinear Fourier analysis

We provide an example of a surface wave elevation with a duration of 600 s generated by JONSWAP spectrum with $\alpha = 0.02$, $\gamma = 3.3$, $f_p = 1/7$Hz and its complex envelope, as shown in Fig. 2a and Fig. 2b, respectively. The blue line is the complex envelope calculated from the Hilbert transform. You can find a more detailed view of the elevation and envelope that is obtained by zooming in from 200 s to 400 s in Fig. 2c. The complex envelope will be analyzed by the nonlinear Fourier transform with vanishing boundary conditions. The nonlinear Fourier spectrum is shown in Fig. 3. Fig. 3a shows the continuous spectrum with ζ on the x-axis and the reflection coefficient on the y-axis. Fig. 3b shows the discrete spectrum with the real part of the eigenvalue on the x-axis representing soliton velocity and the imaginary part on the y-axis representing soliton amplitude. The number of solitons N is 64 in this case. Note that the soliton of the NLS equation in deep water conditions is in the envelope instead of the surface elevation.

Fig. 4 shows the magnitude of the initial complex envelope and the magnitude of envelope of nonlinear spectral components reconstructed by the iNFT. We see that the envelope reconstructed from the full (i.e., continuous and discrete) nonlinear spectrum (orange line) is identical to the initial magnitude of complex envelope (blue line), as shown in Fig. 4a. Fig. 4b and c show the magnitude recovered from only the continuous spectrum (radiation part) and only the discrete spectrum (soliton part), respectively. It is clear that the soliton components dominante the wave field, as most envelope peaks in the time series match the peaks of the initial complex envelope. Meanwhile, Fig. 4d shows the linear sum of time series that correspond to only the continuous spectrum and only the discrete spectrum. It is found that the linear sum of soliton and radiation waves is different from the inverse of the full nonlinear spectrum. This reveals that the nonlinear interaction between continuous spectrum and discrete spectrum cannot be neglected in this case. The soliton energy ratio is 91% in this case, indicating a sea state in a soliton gas-like condition.

TABLE 1: DEFINITION OF FOUR CLASSES

Class	Range
Radiation wave dominance	$E_{\text{sol\_ratio}} < 40\%$
Radiation wave and soliton combination	$40\% \leq E_{\text{sol\_ratio}} < 60\%$
Soliton dominance	$60\% \leq E_{\text{sol\_ratio}} < 90\%$
Soliton gas-like	$90\% \leq E_{\text{sol\_ratio}} < 100\%$

TABLE 2: FOUR CLASSES OF SEA STATES

Length of time series= 600 s Classes	$T_p = 5s$	$T_p = 7s$	$T_p = 9s$	$T_p = 11s$	$T_p = 13s$	$T_p = 15s$	Total
Radiation wave dominance	3%	4%	6%	8%	10%	12%	7%
Radiation wave and soliton combination	4%	6%	8%	10%	12%	13%	9%
Soliton dominance	49%	67%	77%	80%	78%	75%	71%
Soliton gas-like	44%	22%	9%	2%	0%	0%	13%
Length of time series= 1200 s Classes	$T_p = 5s$	$T_p = 7s$	$T_p = 9s$	$T_p = 11s$	$T_p = 13s$	$T_p = 15s$	Total
Radiation wave dominance	1%	1%	2%	3%	4%	5%	3%
Radiation wave and soliton combination	2%	3%	5%	5%	5%	6%	4%
Soliton dominance	26%	35%	48%	54%	60%	70%	49%
Soliton gas-like	72%	60%	45%	38%	32%	19%	44%

4. RESULTS

Soliton energy ratios of JONSWAP models

We investigate how dominant the soliton energy in the wave field is for surface elevation time series generated by the JONSWAP model with random phases, as explained in Sec. 2. There are 9180 JONSWAP spectra in total, with 1530 spectra for each peak period. We generate two sets of surface wave elevation, one for each time duration, 600 s and 1200 s. For each JONSWAP spectrum, we generate 10 time series of surface wave elevations with random phases, resulting in a total of 183600 surface wave elevations. The nonlinear Fourier spectra are then derived from the normalized complex envelopes of these time series. We would like to emphasize again that the NLS solitons in deep water are the envelope solitons instead of the solitary waves described in shallow water.

The energy of solitons and radiation waves and the soliton energy ratio are calculated using the formulas provided in Sec. 3. The soliton energy ratio in this study is the mean soliton energy ratio of the 10 surface wave elevation data. Fig. 5 and Fig. 6 show the mean soliton energy ratio over the JONSWAP parameters α and γ for the time series with durations of 600 s and 1200 s, respectively. Different values of the peak period of the JONSWAP spectra are considered separately from short waves to long waves

Recall that the nonlinear Fourier spectra are classified into four types: radiation wave dominance, radiation wave and soliton combination, soliton dominance, and soliton gas. The classification is based on the soliton energy ratio (see Table 1). First, we direct our attention to Fig. 5. In terms of the distribution of the soliton energy ratio, the spectra with radiation wave dominance (blue dots) are distributed in the region with smaller α. The area with smaller γ has more spectra with radiation wave dominance (blue dots). The spectra with radiation wave and soliton combination (cyan and green dots) are distributed on the right of the radiation wave dominance cases with larger α. Most of the spectra with soliton dominance (orange dots) are distributed right of the radiation wave and soliton combination with larger α. These soliton-dominant cases are the majority of the simulated spectra. The spectra of soliton gas-like cases (yellow dots) are distributed in the right-up region with large α and γ. With regard to the peak periods, the spectra with longer peak periods also have more cases with radiation wave dominance and radiation wave and soliton combination conditions. The spectra with shorter peak periods have more soliton gas cases. By comparing the results of the soliton energy ratio calculated from two sets of time series with durations of 600 s and 1200 s, as shown in Fig. 5 and Fig. 6, we observe that the overall soliton energy ratio is higher in the case of the 1200 s time series. This is attributed to the nonlinear nature of the NFT, for which scaling a signal in time is essentially equivalent to scaling it in amplitude [28, Sec. IV.D-4]. This behavior can already be observed for simple rectangular bores. When the duration is large, the bore will be dominated by solitons [29, Sec. III]. The almost complete reconstruction of a bore from its 23 soliton components is demonstrated in [2, Sec. 7.3].

Table 2 illustrates the occurrence of four classes based on the soliton energy ratio of two sets of surface waves data with different values of peak periods from 5 s to 15 s with an interval of 2 s. The percentage of four classes with radiation wave dominance, equal combination of radiation wave and soliton, soliton dominance and soliton gas-like based on data with a time length of 600 s accounts for 7%, 9%, 71%, and 13%, respectively. The percentage of four classes of data with a time length of 1200 s accounts for 3%, 4%, 49%, and 44%, respectively. If we sum up the percentage of spectra with soliton dominance and soliton gas-like, they are up to

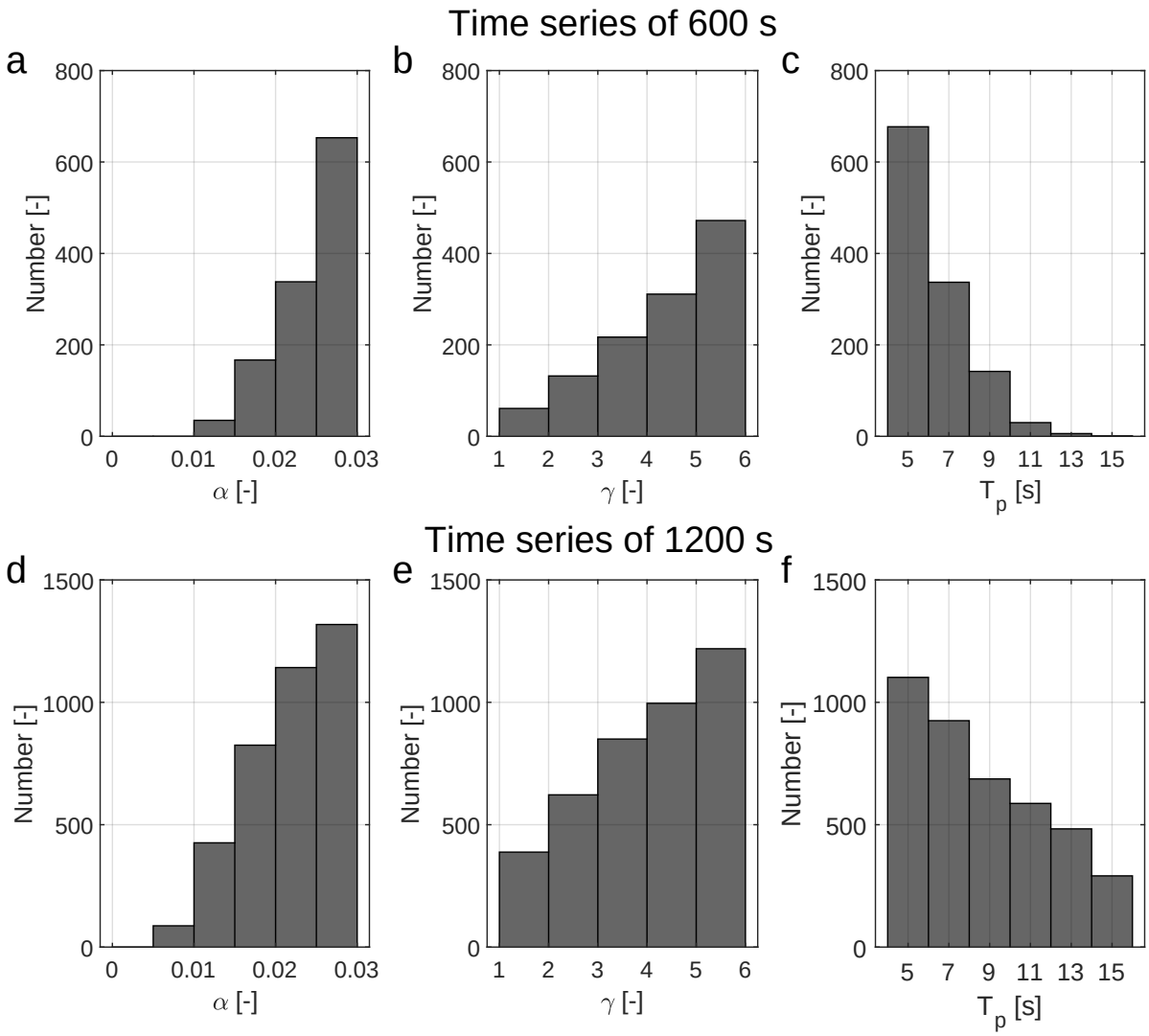

FIGURE 7: HISTOGRAM OF JONSWAP PARAMETERS IN SOLITON GAS-LIKE SEA STATES FOR SURFACE WAVES WITH A TIME LENGTH OF 600 s AND 1200 s. DISTRIBUTION OF α, γ AND T_p FOR SURFACE WAVES WITH A TIME LENGTH OF 600 s IS SHOWN IN FIG. 7A, 7B AND 7C, RESPECTIVELY. AND DISTRIBUTION OF α, γ AND T_p FOR SURFACE WAVES WITH A TIME LENGTH OF 1200 s IS SHOWN IN FIG. 7D, 7E AND 7F, RESPECTIVELY.

84% and 93% for two sets, which account for a high proportion in our simulations. This high percentage might seem surprising, but similar observations have been made in the area of optical fiber communications, where it was found that "linear" communication signals can nevertheless be dominated by solitons [30–32]. If we consider the spectra from short peak period 5 s to long peak period 15 s, it is found that the percentage of radiation wave dominated spectra is increasing, the percentage of spectra of radiation wave and soliton combination is increasing, and the percentage of spectra of soliton gas is decreasing. This suggests that sea states with soliton dominance and soliton gas-like sea states tend to appear in shorter peak period conditions.

Interestingly, if we compare the soliton energy ratio in Fig. 5 and Fig. 6 to the significant wave height in Fig. 1, the spectra with $H_s < 5$m (dark blue dots) in Fig. 1 can correspond to any classes according to the soliton energy ratio in Fig. 5 and Fig. 6. This indicates that the total energy does not determine how dominant the soliton energy is in the whole system. However, the spectra with larger significant wave heights (right-up region) are likely related to the conditions with higher soliton energy ratio. The larger significant wave heights of JONSWAP spectra occur as a result of the shapes of JONSWAP spectra with longer peak period, larger α and larger γ. Our results show that the shapes of JONSWAP spectra actually affect the of soliton energy ratio.

As we mentioned in Section 2, our dataset of the simulated JONSWAP sea states differs from realistic sea states. Several studies discuss the selection of JONSWAP parameters based on in situ measurements [33, 34]. If we follow the joint probability of JONSWAP parameters from the sea in the north of Colombia by Rueda-Bayona et al. (2020) [34], the approximate range with higher probability of JONSWAP parameters is located in $\{0 < \alpha < 0.01$ and $0 < \gamma < 3\}$, $\{0 < \alpha < 0.005$ and $3 < \gamma < 6\}$, and

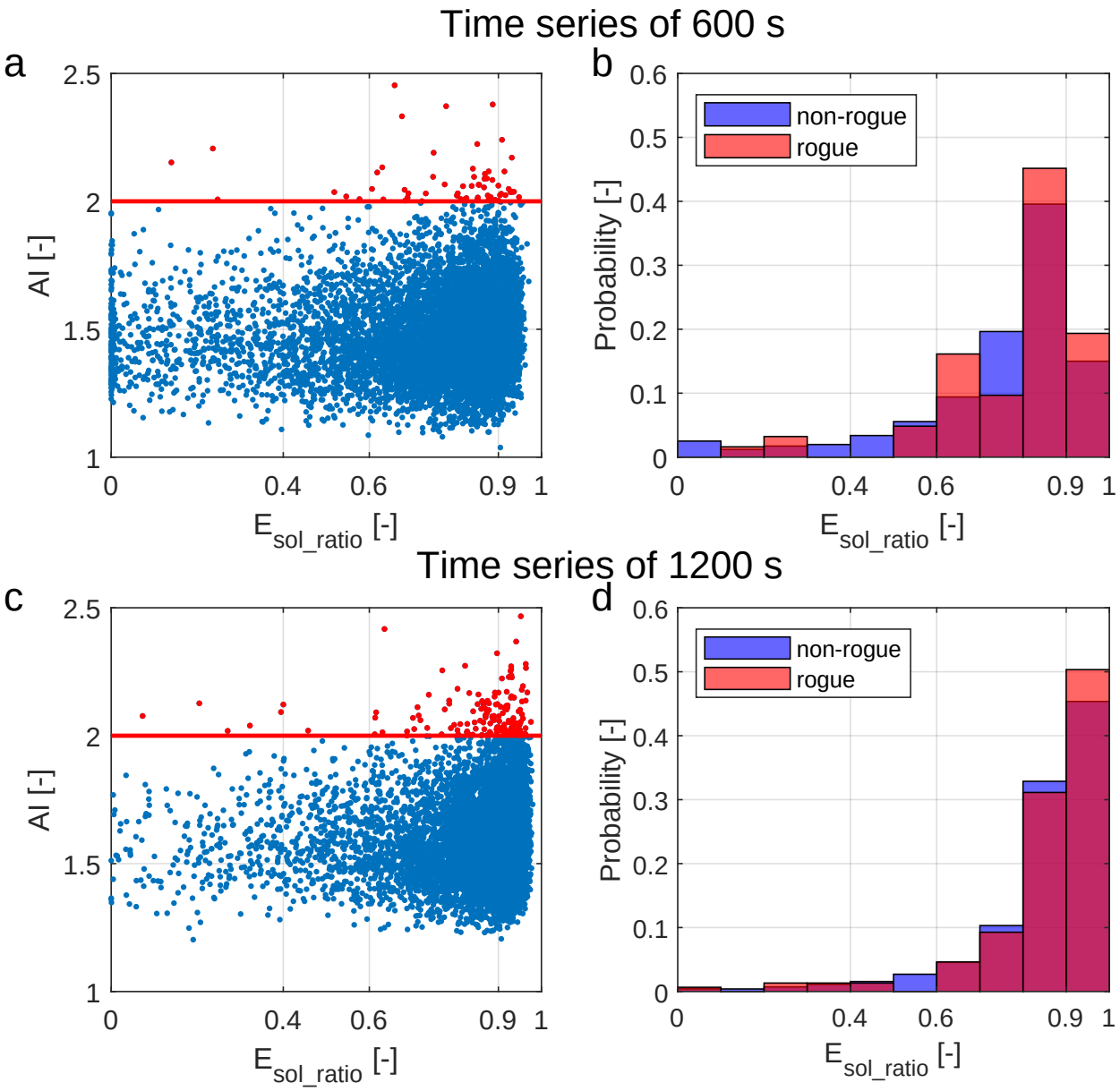

FIGURE 8: COMPARISON BETWEEN NON-ROGUE WAVES AND ROGUE WAVES. A. SCATTER PLOT OF SOLITON ENERGY RATIO VERSUS ABNORMALITY INDEX (AI) FOR SURFACE WAVE DATA WITH A TIME LENGTH OF 600 s. THE RED LINE REPRESENTS THE ROGUE WAVE THRESHOLD, WHICH SEPARATES ALL DATA INTO NON-ROGUE WAVES (BLUE DOTS) AND ROGUE WAVES (RED DOTS). B. HISTOGRAM OF PROBABILITY DENSITY FOR NON-ROGUE WAVES (BLUE BARS) AND ROGUE WAVES (RED BARS) FOR SURFACE WAVE DATA WITH A TIME LENGTH OF 600 s. C. SCATTER PLOT OF SOLITON ENERGY RATIO VERSUS ABNORMALITY INDEX (AI) FOR SURFACE WAVE DATA WITH A TIME LENGTH OF 1200 s. THE RED LINE REPRESENTS THE ROGUE WAVE THRESHOLD, WHICH SEPARATES ALL DATA INTO NON-ROGUE WAVES (BLUE DOTS) AND ROGUE WAVES (RED DOTS). D. HISTOGRAM OF PROBABILITY DENSITY FOR NON-ROGUE WAVES (BLUE BARS) AND ROGUE WAVES (RED BARS) FOR SURFACE WAVE DATA WITH A TIME LENGTH OF 1200 s.

$\{0.01 < \alpha < 0.02$ and $0 < \gamma < 2\}$. In Fig. 5, these ranges mostly belong to the classes of radiation wave dominance and radiation wave and soliton combination.

JONSWAP spectral characteristics of the soliton gas-like sea states

We now focus on the soliton gas-like case ($90\% \leq E_{\text{sol\_ratio}}$). In our simulation, the soliton gas-like sea states with a time length of 600 s account for 13% of the 9180 spectra in total. The number of soliton gas-like spectra from the peak period of 5 s to 15 s is 677, 337, 142, 30, 6, and 1, respectively. The soliton gas-like sea states with a time length of 1200 s account for 44% of the 9180 spectra in total. The number of soliton gas-like spectra from the peak period of 5 s to 15 s is 1102, 925, 687, 587, 483, and 291, respectively. The distribution of the JONSWAP parameters for soliton gas-like sea states is shown in Fig. 7. As you can see in

Fig. 7a, the soliton gas-like sea states with a time length of 600 s occur in the range of α from 0.01 to 0.03. It can be seen that increasing α leads to an increase in the number of soliton gas-like spectra. Note that soliton gas-like sea states are not observed when the Phillip's parameter α is less than 0.01. According to the distribution of the peak enhancement parameter γ of soliton gas-like sea states in Fig. 7b, the soliton gas-like sea states occur in full range of γ from 1 to 6. However, the number of soliton gas-like sea states increases with increasing peak enhancement parameter γ. Meanwhile, shorter peak periods have more soliton gas-like sea states, as shown in 7c. There are 97% of soliton gas-like sea states with peak period lower than 11 s in our simulation. For the soliton gas-like sea states with a time length of 1200 s, as shown in Fig. 7d, they occur in the range of α from 0.005 to 0.03. Most of soliton gas-like sea states (98%) are observed when the Phillip's parameter α is larger than 0.01. The distribution of the peak enhancement parameter γ of soliton gas-like sea states in Fig. 7e has similar results that more cases of soliton gas-like sea states occur with larger peak enhancement parameter γ. As shown in Fig. 7f, the shorter peak periods have more soliton gas-like sea states. The above results indicate that a larger α leading to more energy in the system, a larger γ leading to more energy concentration in the peak, and a shorter peak period are related to the soliton gas-like sea states.

Sea states with rogue waves

In [9], rogue waves emerging in soliton gases due to collisions of solitons were observed. Next, we therefore investigate the occurrence of rogue waves with respect to the soliton energy ratio. A rogue wave is a wave with a wave height larger than twice the significant wave height $H_{1/3}$. The abnormality index (AI) is defined as the ratio between the maximum wave height $H_{\max}$ and the significant wave height $H_{1/3}$. We generate one time series with random phases for each JONSWAP spectra, in total 9180 time series. We show the relation between the soliton energy ratio and AI with a time length of 600 s in Fig. 8a and with a time length of 1200 s in Fig. 8c. The red line is the rogue wave threshold $AI = 2$. The data with $AI > 2$ are considered rogue waves (red dots). The data with $AI \leq 2$ are non-rogue waves (blue dots). There are totally 62 rogue wave data in whole 9180 data set with a time length of 600 s and 151 rogue wave data in whole 9180 data set with a time length of 1200 s.

We classify these rogue wave data into four types, as shown in Table 3. The four classes from radiation wave dominance, radiation wave and soliton combination, soliton dominance to soliton gas-like conditions account for 5%, 5%, 71%, 19% of all rogue-wave time series with length of 600 s, respectively. And the four classes account for 3%, 1%, 45%, 51% of all rogue-wave time series with length of 1200 s, respectively. Clearly, most rogue waves time series (90% for time series with length of 600 s and 96% for time series with length of 1200 s) have a high soliton energy ratio (60% or more). Upon analysis, it shows that the probability of rogue wave occurrences under soliton gas-like conditions is higher in datasets with a length of 1200 seconds (51%) in comparison to those with a length of 600 seconds (19%).

If we compare the distribution of the soliton energy ratio for rogue wave data (red bars) with non-rogue wave data (blue bars), as shown in Fig. 8b and Fig. 8d, we find that the probability of rogue waves is only slightly increased under soliton gas-like conditions. This finding can also be seen in Table 3. In time series of 600 s, 15% of the non-rogue waves are classified as soliton gases, while the percentage is higher at 19% for rogue waves. Similarly, in time series of 1200 s, 45% of the non-rogue waves are classified as soliton gases, while the percentage is higher at 51% for rogue waves. However, the above analysis does not consider wave evolution. Therefore, further investigation is needed to determine the occurrence of rogue waves after propagating a certain distance with soliton energy ratio.

TABLE 3: CLASSIFICATION OF THE NON-ROGUE AND ROGUE WAVE DATA BASED ON THE SOLITON ENERGY RATIO

Length of time series= 600 s Classes	Non-rogue	Rogue
Radiation wave dominance	7%	5%
Radiation wave and soliton combination	9%	5%
Soliton dominance	69%	71%
Soliton gas-like	15%	19%
Length of time series= 1200 s Classes	**Non-rogue**	**Rogue**
Radiation wave dominance	3%	3%
Radiation wave and soliton combination	4%	1%
Soliton dominance	48%	45%
Soliton gas-like	45%	51%

5. CONCLUSIONS

In this work, we investigated what kind of JONSWAP spectra lead to soliton gases in deep water conditions. We used the nonlinear Fourier transform (NFT) based on the nonlinear Schrödinger (NLS) equation for the analysis of surface waves. We generated 183600 surface wave time series with two sets of time durations of 600 s and 1200 s from 9180 JONSWAP spectra for which the Phillip's parameter ranged from 0.001 to 0.03, the peak enhancement parameter γ from 1 to 6, and the peak period T_p with from 5 s to 15 s. Based on the nonlinear Fourier spectra obtained from nonlinear analysis, we found that the majority of data fall into the soliton dominance and soliton gas-like categories. Higher values of α, higher values of γ and shorter peak periods contribute to the occurance of soliton gas-like sea states. We then studied sea states that contained rogue waves. We found that 90% and 96% of the rogue waves in our data sets with time lengths of 600s and 1200s exist, respectively, in sea states with soliton dominance and soliton gas-like conditions. For non-rogue waves, the corresponding numbers were 84% and 93%. The probability of rogue waves is thus slightly higher compared to that of non-rogue waves under soliton gas-like conditions. The distribution of the JONSWAP parameters however does not reflect their probability of occurrence for real sea conditions in the field. For future study, it would be interesting to assess how dominant solitons are for realistic JONSWAP parameters.

REFERENCES

[1] Brühl, Markus and Oumeraci, Hocine. "Analysis of long-period cosine-wave dispersion in very shallow water using nonlinear Fourier transform based on KdV equation." *Applied Ocean Research* Vol. 61 (2016): pp. 81–91.

[2] Brühl, Markus, Prins, Peter J, Ujvary, Sebastian, Barranco, Ignacio, Wahls, Sander and Liu, Philip L-F. "Comparative analysis of bore propagation over long distances using conventional linear and KdV-based nonlinear Fourier transform." *Wave Motion* Vol. 111 (2022): p. 102905.

[3] Zabusky, Norman J and Kruskal, Martin D. "Interaction of" solitons" in a collisionless plasma and the recurrence of initial states." *Physical review letters* Vol. 15 No. 6 (1965): p. 240.

[4] Novikov, S, Manakov, Sergei V, Pitaevskii, Lev Petrovich and Zakharov, Vladimir Evgenevič. *Theory of solitons: the inverse scattering method*. Springer Science & Business Media (1984).

[5] Gardner, Clifford S, Greene, John M, Kruskal, Martin D and Miura, Robert M. "Method for solving the Korteweg-deVries equation." *Physical review letters* Vol. 19 No. 19 (1967): p. 1095.

[6] Shabat, Aleksei and Zakharov, Vladimir. "Exact theory of two-dimensional self-focusing and one-dimensional self-modulation of waves in nonlinear media." *Sov. Phys. JETP* Vol. 34 No. 1 (1972): p. 62.

[7] Ablowitz, Mark J, Kaup, David J, Newell, Alan C and Segur, Harvey. "The inverse scattering transform-Fourier analysis for nonlinear problems." *Studies in Applied Mathematics* Vol. 53 No. 4 (1974): pp. 249–315.

[8] Boffetta, Guido and Osborne, Alfred Richard. "Computation of the direct scattering transform for the nonlinear Schrödinger equation." *Journal of computational physics* Vol. 102 No. 2 (1992): pp. 252–264.

[9] Gelash, AA and Agafontsev, DS. "Strongly interacting soliton gas and formation of rogue waves." *Physical Review E* Vol. 98 No. 4 (2018): p. 042210.

[10] Zakharov, VE. "Kinetic equation for solitons." *Sov. Phys. JETP* Vol. 33 No. 3 (1971): pp. 538–540.

[11] El, GA and Kamchatnov, AM. "Kinetic equation for a dense soliton gas." *Physical review letters* Vol. 95 No. 20 (2005): p. 204101.

[12] El, Gennady A. "Critical density of a soliton gas." *Chaos: An Interdisciplinary Journal of Nonlinear Science* Vol. 26 No. 2 (2016): p. 023105.

[13] Costa, Andrea, Osborne, Alfred R, Resio, Donald T, Alessio, Silvia, Chriv ' i, Elisabetta, Saggese, Enrica, Bellomo, Katinka and Long, Chuck E. "Soliton turbulence in shallow water ocean surface waves." *Physical review letters* Vol. 113 No. 10 (2014): p. 108501.

[14] Redor, Ivan, Barthélemy, Eric, Michallet, Hervé, Onorato, Michael and Mordant, Nicolas. "Experimental evidence of a hydrodynamic soliton gas." *Physical Review Letters* Vol. 122 No. 21 (2019): p. 214502.

[15] Suret, Pierre, Tikan, Alexey, Bonnefoy, Félicien, Copie, François, Ducrozet, Guillaume, Gelash, Andrey, Prabhudesai, Gaurav, Michel, Guillaume, Cazaubiel, Annette, Falcon, Eric et al. "Nonlinear spectral synthesis of soliton gas in deep-water surface gravity waves." *Physical Review Letters* Vol. 125 No. 26 (2020): p. 264101.

[16] Hasselmann, Klaus, Barnett, Tim P, Bouws, E, Carlson, H, Cartwright, David E, Enke, K, Ewing, JA, Gienapp, A, Hasselmann, DE, Kruseman, P et al. "Measurements of wind-wave growth and swell decay during the Joint North Sea Wave Project (JONSWAP)." *Supplement to the German Hydrographic Journal, Series A* (1973).

[17] Medina, Josep R and Hudspeth, RT. "A review of the analyses of ocean wave groups." *Coastal Engineering* Vol. 14 No. 6 (1990): pp. 515–542.

[18] Wahls, Sander, Bruehl, Markus, Fan, Yang-Ming and Huang, Ching-Jer. "Nonlinear Fourier Analysis of Free-Surface Buoy Data Using the Software Library FNFT." *International Conference on Offshore Mechanics and Arctic Engineering*, Vol. 84386: p. V06BT06A070. 2020. American Society of Mechanical Engineers.

[19] Zakharov, Vladimir E. "Stability of periodic waves of finite amplitude on the surface of a deep fluid." *Journal of Applied Mechanics and Technical Physics* Vol. 9 No. 2 (1968): pp. 190–194.

[20] Hasimoto, Hidenori and Ono, Hiroaki. "Nonlinear modulation of gravity waves." *Journal of the Physical Society of Japan* Vol. 33 No. 3 (1972): pp. 805–811.

[21] Hasegawa, Akira and Matsumoto, Masayuki. "Optical solitons in fibers." *Optical Solitons in Fibers*. Springer (2003): pp. 41–59.

[22] Karpman, Vladimir Iosifovich. *Non-linear waves in dispersive media: International series of monographs in natural philosophy*. Vol. 71. Elsevier (2016).

[23] Ablowitz, Mark J and Segur, Harvey. *Solitons and the inverse scattering transform*. SIAM (1981).

[24] Osborne, AR and Bergamasco, L. "The solitons of Zabusky and Kruskal revisited: Perspective in terms of the periodic spectral transform." *Physica D: Nonlinear Phenomena* Vol. 18 No. 1-3 (1986): pp. 26–46.

[25] Lee, Yu-Chen, Wahls, Sander and Brühl, Markus. "Evaluation of Nonlinear Fourier-Based Maximum Wave Height Predictors Under the Nonlinear Schrödinger Equation." *International Conference on Offshore Mechanics and Arctic Engineering*, Vol. 85901: p. V05BT06A060. 2022. American Society of Mechanical Engineers.

[26] Ablowitz, Mark J, Ablowitz, MA, Prinari, B and Trubatch, AD. *Discrete and continuous nonlinear Schrödinger systems*. Vol. 302. Cambridge University Press (2004).

[27] Wahls, Sander, Chimmalgi, Shrinivas and Prins, Peter J. "FNFT: A software library for computing nonlinear Fourier transforms." *Journal of Open Source Software* Vol. 3 No. 23 (2018): p. 597.

[28] Yousefi, Mansoor I and Kschischang, Frank R. "Information transmission using the nonlinear Fourier transform, Part I: Mathematical tools." *IEEE Transactions on Information Theory* Vol. 60 No. 7 (2014): pp. 4312–4328.

[29] Gelash, Andrey, Agafontsev, Dmitry, Suret, Pierre and Randoux, Stéphane. "Solitonic model of the condensate." *Physical Review E* Vol. 104 No. 4 (2021): p. 044213.

[30] Wahls, Sander, Le, Son T, Prilepsk, Jaroslaw E, Poor, H Vincent and Turitsyn, Sergei K. "Digital backpropagation in the nonlinear Fourier domain." *2015 IEEE 16th International Workshop on Signal Processing Advances in Wireless Communications (SPAWC)*: pp. 445–449. 2015. IEEE.

[31] Sedov, Egor V, Redyuk, Alexey A, Fedoruk, Mikhail P, Gelash, Andrey A, Frumin, Leonid L and Turitsyn, Sergey K. "Soliton content in the standard optical OFDM signal." *Optics Letters* Vol. 43 No. 24 (2018): pp. 5985–5988.

[32] De Koster, Pascal and Wahls, Sander. "Dispersion and nonlinearity identification for single-mode fibers using the nonlinear Fourier transform." *Journal of Lightwave Technology* Vol. 38 No. 12 (2020): pp. 3252–3260.

[33] Boukhanovsky, AV and Soares, C Guedes. "Modelling of multipeaked directional wave spectra." *Applied Ocean Research* Vol. 31 No. 2 (2009): pp. 132–141.

[34] Rueda-Bayona, Juan Gabriel, Guzmán, Andrés and Cabello Eras, Juan José. "Selection of JONSWAP spectra parameters During Water-depth and Sea-state Transitions." *Journal of Waterway, Port, Coastal, and Ocean Engineering* Vol. 146 No. 6 (2020): p. 04020038.